Available online at www.sciencedirect.com
SCIENCE DIRECT®
Journal of Power Sources 137 (2004) 30–42
JOURNAL OF POWER SOURCES
www.elsevier.com/locate/jpowsour

Fuel cell modelling for building cogeneration applications

Alex Ferguson [a,*], V. Ismet Ugursal [b]

[a] CANMET Energy Technology Centre, Natural Resources Canada, Ottawa, Ont., Canada
[b] Department of Mechanical Engineering, University of Victoria, Victoria, BC, Canada

Received 5 April 2004; accepted 3 May 2004
Available online 10 August 2004

Abstract

Fuel cell technologies are an emerging alternative to combustion-based cogeneration and traditional, centralized power generation. To accurately size fuel cell systems for houses and predict their performance, a system model that can be integrated into existing building simulation tools is required. A steady-state model of a generic PEM cogeneration fuel cell system was developed to fill this need. The model is useful for (i) estimating system fuel use, and electrical and thermal production, (ii) investigating the suitability of fuel cell systems in different climates, (iii) sizing fuel cell systems and ancillary equipment, and (iv) evaluating different control strategies. The model has been validated using empirical data and published estimates produced with other models. In this paper, the development of the model and the results of these validation studies are discussed. Also, the results from a Canadian case study investigating the effect of varying fuel cell size on the performance of a cogeneration system are presented.

Keywords: Residential fuel cell system; Cogeneration; Building simulation

1. Introduction

Fuel cell systems have received increasing attention in recent years as a viable alternative for meeting the electrical and thermal needs of buildings. Operational fuel cell systems have demonstrated superior performance to combustion-based generation technologies at scales from 5 kW to 2 MW [17], a range that includes the electrical requirements of most buildings. Today, proton exchange membrane (PEM) fuel cell and solid oxide fuel cell (SOFC) technologies are in demonstration and pre-commercialization phases in portable power generation, static power generation, cogeneration, and transportation applications. Once commercially available, it is anticipated that efficient natural gas fuel cell technology will offer an economically and environmentally attractive alternative to both combustion cogeneration plants and centralized power generation [4].

Since small to medium-scale stationary fuel cell systems can convert 40–50% of the fuel's chemical energy to electricity (based on lower heating value), exploiting the coincident thermal output can substantially improve the overall system efficiency. Therefore, building simulation technology, which characterizes the interactions between the environment, building envelope, mechanical systems, and occupants, is a valuable tool for studying these complex systems.

As researchers, policy-makers, manufacturers, and homebuilders consider the suitability of fuel cell systems in residential and commercial markets, there exists a need for a modelling tool capable of accurately predicting the interactions between fuel cell systems and buildings in cogeneration applications. Such a tool would be useful in (i) estimating fuel cell system energy production and fuel use in static cogeneration applications, (ii) determining the suitability of fuel cell systems in different climates and building types, (iii) determining the optimal size of a fuel cell system for a given application, and (iv) evaluating different system architectures and control strategies for fuel cell systems.

In this project, a PEM fuel cell component model (PFCCM) was developed and integrated into the ESP-r simulation program.[1] The model has been validated using empirical data and the results from other fuel cell modelling studies, and was used to investigate the performance of PEM fuel cell systems in a representative Canadian household.

In the present paper, the development and validation of the PFCCM are presented, followed by results obtained using

* Corresponding author. Tel.: +1 613 995 3294.
E-mail address: aferguso@nrcan.gc.ca (A. Ferguson).

[1] Energy Systems Research Unit, University of Strathclyde, 75 Montrose Street, Glasgow G1 1XJ, UK. Tel.: +44 141 548 3986; fax: +44 552 5105.esru@strath.ac.uk.

0378-7753/$ – see front matter © 2004 Published by Elsevier B.V.
doi:10.1016/j.jpowsour.2004.05.021

the PFCCM to investigate the effects of fuel cell system sizing in a Canadian case study.

2. Overview of PEM fuel cell technology

A natural gas PEM fuel cell system is comprised of (i) a fuel cell stack, in which the chemical energy contained in hydrogen is converted into electricity, (ii) a fuel processor, which converts the hydrocarbon fuel into a hydrogen-rich mixture that can be used in the stack, (iii) heat recovery equipment, and (iv) auxiliary systems, such as compressors and pumps.

2.1. Fuel cell stack

A fuel cell stack is a collection of anode–electrolyte–cathode structures, in which electrochemical reactions occur. The construction and operation of a fuel cell stack is similar to that of a battery, except that reactants and products flow continuously through a fuel cell.

PEM fuel cell systems operate at low temperature (50–90 °C), and are fueled using hydrogen or natural gas that has been converted to a mixture of hydrogen and carbon dioxide. The reactions occurring in a PEM fuel cell stack proceed as follows:

$$\text{Anode} : \mathrm{H_2} \rightarrow 2\mathrm{H^+} + 2\mathrm{e^-} \tag{1}$$

$$\text{Cathode} : 2\mathrm{H^+} + \tfrac{1}{2}\mathrm{O_2} + 2\mathrm{e^-} \rightarrow \mathrm{H_2O} \tag{2}$$

$$\text{Overall} : \mathrm{H_2} + \tfrac{1}{2}\mathrm{O_2} \rightarrow \mathrm{H_2O} \tag{3}$$

The electrochemical efficiency of the fuel cell stack (η_{cell}) is described by the ratio between the stack voltage (V_{cell}) and oxidation potential (V_{ox}):[2]

$$\eta_{\text{cell}} = \frac{V_{\text{cell}}}{V_{\text{ox}}} \tag{4}$$

The theoretical maximum amount of electrical energy that may be recovered from the electrochemical reactions occurring within the fuel cell stack is equal to the change in the Gibbs free energy occurring within the stack. The total amount of energy released in the electrochemical reactions is equal to the enthalpy change within the cell. Thus, the theoretical maximum efficiency of conversion from chemical to electrical energy (η_{max}) is the ratio between the change in the Gibbs free energy (ΔG_{cell}) and the change in the enthalpy (ΔH_{cell}):

$$\eta_{\text{max}} = \frac{\Delta G_{\text{cell}}}{\Delta H_{\text{cell}}} \tag{5}$$

The Second Law of Thermodynamics requires that the theoretical maximum efficiency can be obtained only when the cell operates under reversible conditions, and these conditions are approached when there is no electrical load on the cell. The fuel cell stack voltage under reversible conditions (V_{rev}) can be calculated by multiplying the oxidation potential by the maximum theoretical efficiency:

$$V_{\text{rev}} = \eta_{\text{max}} V_{\text{ox}} \tag{6}$$

Inefficiencies associated with the electrochemical reactions, called polarization losses, lower the overall cell efficiency under loaded conditions. Three types of polarization losses exist:

- activation polarizations that result from the electrochemical barriers tha oppose current and ion flow,
- concentration polarizations that result from local depletion of the reactants on the electrodes, and
- ohmic polarizations that result from electrical resistances within the cell.

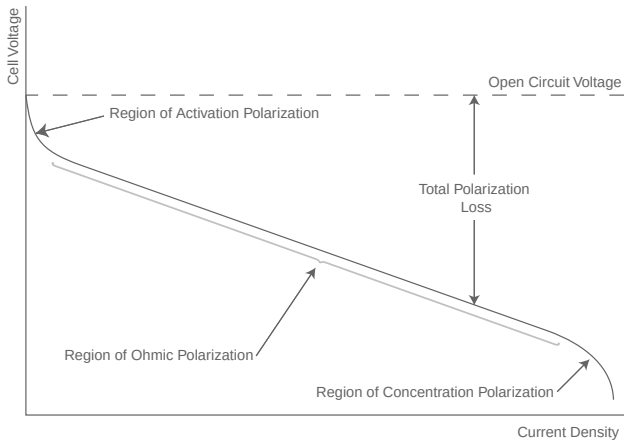

Fig. 1. Arbitrary fuel cell polarization curve. Adapted from Hirschenhofer [9].

Fig. 1 depicts an arbitrary fuel cell polarization curve. The cell voltage is plotted on the vertical axis, and the cell current density is plotted on the horizontal axis. As the cell electrical power output increases, polarization losses lower the cell voltage. Activation polarization losses increase rapidly as the stack load increases from zero but then quickly approach a constant value. Conversely, concentration polarization losses are only significant under high current loadings. In the region where the activation polarization losses are effectively constant and the concentration polarization losses are negligible, the curve is characterized entirely by ohmic polarization losses. Since ohmic polarization losses are a linear function of the current, the polarization curve displays linear behavior through this region, called the *Tafel* region. The voltage–current characteristics of real fuel cell systems exhibit the linear behavior of the Tafel region over the system operating range because the activation and concentration polarization regions are normally unsuitable for fuel cell operation [8,16].

[2] 1.48 V, based on the higher heating value (HHV) of the fuel.

The inefficiencies associated with the electrochemical reactions also produce a substantial amount of heat. In PEM fuel cell systems, this heat must be extracted by heat-recovery equipment or an auxiliary cooling system to prevent the stack temperature from rising above its efficient operating range.

2.2. Fuel processor

The fuel processor is used to convert a hydrocarbon fuel, such as natural gas, into a stream containing hydrogen that may be oxidized in the fuel cell stack. A fuel processor is typically comprised of four separate reaction vessels:

Reformer: The hydrocarbon and steam streams first pass through a high temperature reactor vessel called a reformer where most of the fuel is converted into hydrogen and carbon monoxide. Some of the carbon monoxide produced in the reformer may also react with water to form carbon dioxide. Natural gas reformers typically operate at temperatures over 700 °C [9].

High temperature water shift reactor: The high temperature water shift reactor (HTWS) is used to convert carbon monoxide to carbon dioxide. The HTWS reactor typically operates at temperatures between 260 and 320 °C [9].

Low temperature water shift reactor: The low temperature water shift reactor (LTWS) is used to convert the remaining carbon monoxide to carbon dioxide. The LTWS reactor typically operates at temperatures between 200 and 260 °C [9].

Preferential oxidation reactor (PROX): A preferential oxidation reactor (PROX) is used to shift any remaining carbon monoxide to carbon dioxide by introducing a suitable amount of oxygen to the reformate stream. This is required as trace amounts of carbon monoxide will substantially reduce the performance of the cell stack [9].

Natural gas PEM fuel cell systems also incorporate a burner, in which unused hydrogen and auxiliary fuel are burned to supply the heat required to heat reactants, produce steam and support the endothermic reforming reactions in the fuel processor.

Five separate reactions occur in the fuel processor:

$$C_xH_yO_z + (x - z)\,H_2O \leftrightarrow xCO + \left(x + \frac{y}{2} - z\right)\,H_2 \quad (7)$$

$$CO + H_2O \leftrightarrow CO_2 + H_2 \quad (8)$$

$$CO + 0.5O_2 \leftrightarrow CO_2 \quad (9)$$

$$C_xH_yO_z + \left(x + \frac{y}{4} - \frac{z}{2}\right)\,O_2 \leftrightarrow xCO_2 + \frac{y}{2}\,H_2O \quad (10)$$

$$H_2 + 0.5O_2 \leftrightarrow H_2O \quad (11)$$

Hydrocarbon fuel and high-temperature steam are reacted in the reformer to produce a mixture of hydrogen and carbon monoxide via the reaction pathway described in Eq. (7). Before leaving the reformer, some of the carbon monoxide further reacts with additional water to produce carbon dioxide and hydrogen via the water shift reaction, described by Eq. (8). The resulting reformate is subsequently directed into the HTWS and LTWS reactors, where additional carbon dioxide and hydrogen are produced via the water shift reaction.

The presence of un-reformed fuel and un-converted carbon monoxide in the reformate can substantially reduce the performance of the fuel cell stack. Before the hydrogen-rich reformate can react in the fuel cell stack, these contaminants are reacted with oxygen in the PROX reactor (Eqs. (9) and (10)). Some hydrogen is also converted back to water in this process (Eq. (11)).

2.3. Heat recovery equipment

The fuel and water must be heated to temperatures over 700 °C before they can be reacted in the reformer. Conversely, the hydrogen-rich reformate produced by the fuel processor must be simultaneously cooled to the fuel cell stack operating temperature before it can be reacted in the fuel cell stack. The system's efficiency can be greatly increased if the required heating and cooling is accomplished by transferring heat from the streams requiring cooling to the streams requiring heating. In fuel cell systems, this is accomplished using a network of heat exchangers.

2.4. Auxiliary systems

PEM fuel cell systems also incorporate several ancillary devices necessary for their operation. These devices include:

- pumps that circulate water and liquid fuels,
- compressors that provide high pressure air and gaseous fuel streams,
- electric motors that power the pumps and compressors,
- power conditioning equipment that converts the fuel cell's direct current output into alternating current useful in the building, and
- mechanical cooling equipment that provides supplementary heat extraction required by the fuel cell stack and cooling processes.

3. PEM full cell component model

The PEM fuel cell component model (PFCCM) comprises of (i) an electrochemical model that estimates the performance of the fuel cell stack, (ii) a thermal model that characterizes the energy and mass flows in the fuel processor, and (iii) a heat recovery model that predicts the amount of heat that can be transferred between heating and cooling processes, the amount of auxiliary heat required in the fuel processor, and the amount of surplus heat that can be recovered for space and domestic hot-water heating use. The PFCCM is a steady-state model that is suitable for use in building simulation software, such as ESP-r.

3.1. Electrochemical model

In 2001, Thorstensen published a simplified parametric modelling study of part-load system efficiencies for various fuel cell systems [16]. Thorstensen demonstrated that if the fuel cell stack voltage is assumed to vary linearly with current, the polarization curve may be approximated using a single linear function with the maximum cell potential at zero current (open circuit conditions) and the maximum current occurring at zero cell potential (short circuit conditions). This approach permits calculation of the *part-load efficiency* (η_v) of the cell, which quantifies the inefficiencies associated with activation, concentration, and ohmic polarization losses. The overall cell efficiency may be determined by multiplying the part-load efficiency by the maximum theoretical efficiency:

$$\eta_{\text{cell}} = \eta_{\max}\eta_v \tag{12}$$

Data obtained from experimental fuel cell stacks indicate that activation polarizations remain effectively constant over the fuel cell's operating range [8]. If they are assumed to be constant, the activation polarizations may also be considered in the part-load efficiency calculation. This is accomplished by introducing a parameter, α, that describes the ratio between the constant activation polarization and the theoretical open cell voltage:

$$\alpha = \frac{\Delta V_\alpha}{V_{\text{rev}}} \tag{13}$$

$$\alpha = \frac{V_{\text{rev}} - V_\zeta}{V_{\text{rev}}} \tag{14}$$

where ΔV_α is the reduction in voltage associated with the activation polarization losses, and V_ζ is the voltage, at which the linear approximation to the Tafel region intersects the y-axis.

The introduction of α permits approximation of the fuel cell polarization curve using two linear line segments:

- the first segment is a vertical line starting at the cell open circuit reversible voltage and ending at some point on the vertical axis, and
- the second segment is a diagonal line collinear with the Tafel portion of the polarization curve that starts at the endpoint of the first segment.

The approximated polarization curve is depicted in Fig. 2. The length of the vertical line segment is determined by the amount α, which is the constant approximation of the activation polarization at full load.

Using a method similar to that presented by Thorstensen [16], an expression for the part-load efficiency as a function of the cell electrical power output can be obtained. The cell voltage (V_{cell}) may be expressed as the product of the reversible cell potential (V_{rev}) and the part-load efficiency (η_v):

$$V_{\text{cell}} = \eta_v V_{\text{rev}} \tag{15}$$

Given the idealized, linear voltage–current relationship, it is also possible to express the cell current (I_{cell}) as a function of the part-load efficiency and the short circuit current (I_{sc}):

$$I_{\text{cell}} = I_{\text{sc}}\left(\frac{(1-\alpha)-\eta_v}{1-\alpha}\right) \tag{16}$$

Since the cell electrical power output is the product of voltage and current, Eqs. (15) and (16) may be combined to obtain the cell power as a function of the part-load efficiency:

$$P(\eta_v) = V_{\text{rev}} I_{\text{sc}} \eta_v \left(\frac{(1-\alpha)-\eta_v}{1-\alpha}\right) \tag{17}$$

The maximum theoretical electrical power can be determined by first differentiating Eq. (17) with respect to the

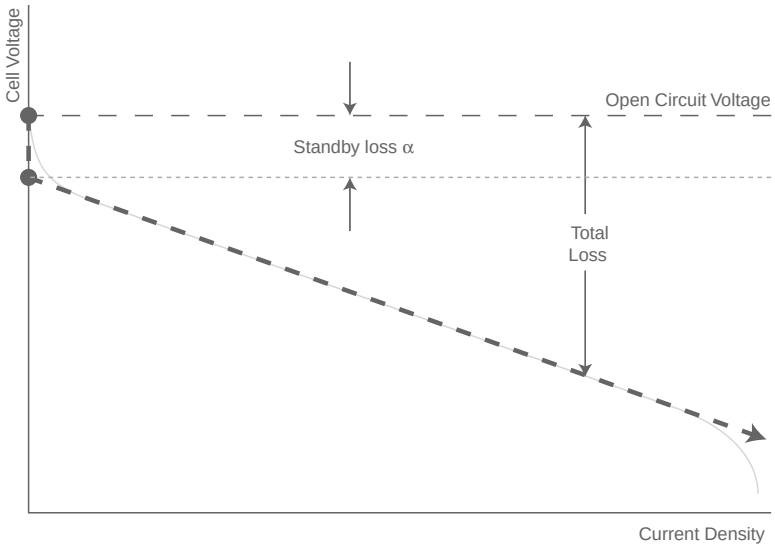

Fig. 2. Simplified fuel cell polarization curve.

part-load efficiency (η_ν) to obtain Eq. (18).

$$P'(\eta_\nu) = V_{\text{rev}} I_{\text{sc}}((1-\alpha) - 2\eta_\nu) \tag{18}$$

If Eq. (18) is set equal to zero, the efficiency at the maximum theoretical electrical power ($\eta_{\nu P_{\max}}$) can be determined. An expression for the maximum theoretical power can also be obtained by substituting this value into Eq. (17):

$$\eta_{\nu P_{\max}} = \frac{1-\alpha}{2} \tag{19}$$

$$P_{\max} = \frac{V_{\text{rev}} I_{\text{sc}}(1-\alpha)}{4} \tag{20}$$

Using Eqs. (16)–(20), a parametric relationship describing the fuel cell stack's part-load efficiency as a function of its gross power output (P_{gross}) may be obtained:

$$\eta_\nu(P) = (1-\alpha)\left(\frac{1+\sqrt{1-(P_{\text{gross}}/P_{\max})}}{2}\right) \tag{21}$$

The value of the theoretical maximum power parameter, described by Eq. (20), may vary from 130 to 180% of the nominal rated output and can be difficult to determine for a given fuel cell system. However, it may be calculated if the stack electrochemical efficiency (ηP_{rated}) under its rated load (P_{rated}) is known:

$$P_{\max} = \frac{P_{\text{rated}}}{1-(2\eta P_{\text{rated}}/(\eta_{\max}(1-\alpha)) - 1)^2} \tag{22}$$

The rate of enthalpy change required within the cell to produce the gross electrical power (P_{gross}) can be determined as follows:

$$\Delta \dot{H}_{\text{cell}} = \frac{P_{\text{gross}}}{\eta_{\text{cell}}} \tag{23}$$

The actual power delivered by the fuel cell, P_{net} can also be determined:

$$P_{\text{net}} = \eta_{\text{pc}} P_{\text{gross}} - P_{\text{para}} \tag{24}$$

where η_{pc} is the nominal efficiency of the power conditioning equipment and P_{para} is the parasitic electrical consumption associated with the system compressors and pumps. As not all of the chemical energy released in the fuel cell stack is converted to electrical work, heat is also produced in the stack. This amount of heat, ($\dot{Q}_{\text{cell}}$), can be determined using the calculated cell conversion efficiency:

$$\dot{Q}_{\text{cell}} = \Delta \dot{H}_{\text{cell}}(1-\eta_{\text{cell}}) \tag{25}$$

To ensure that the fuel cell operates at its optimal temperature, this heat must be extracted from the stack using a heat recovery arrangement or mechanical cooling equipment. The heat extraction from the fuel cell stack is accomplished by passing water though channels in the fuel cell stack. If suitable demand exists, the low-grade surplus heat may be used in space and domestic hot water heating applications. Otherwise, it must be exhausted to the atmosphere using a cooling fan.

3.2. Thermal model

Each reactor in the fuel cell system is modelled as a single control volume. Applying the First Law of Thermodynamics, Eq. (26) is obtained:

$$\sum_{\text{products}} \dot{n}_i\,(h_{\text{f}} + h_{T_{\text{out}}} - h_{\text{STP}})_i = \sum_{\text{reactants}} \dot{n}_i\,(h_{\text{f}} + h_{T_{\text{in}}} - h_{\text{STP}})_i - \dot{Q}_{\text{L}} \tag{26}$$

where $\dot{n}_i$ is the flow rate of species i, $(h_{\text{f}})_i$, is the enthalpy of formation of species i. Symbols $(h(T_{\text{in}}))_i$ and $(h(T_{\text{out}}))_i$ are the enthalpies of species at the reactor inlet and outlet temperatures, respectively. $(h_{\text{STP}})_i$ describes the enthalpy of species at standard temperature and pressure, and $\dot{Q}_{\text{L}}$ quantifies the amount of heat lost from the reactor.

3.3. Heat recovery model

A review of several conceptual and operating fuel cell system schematics [8,3,9] indicated that the required heating and cooling can be accomplished with different arrangements of heat exchangers and fluid paths. A model that explicitly simulated one of these arrangements might be less accurate when other fuel cell systems are considered, and the inherent complication associated with the heat exchanger network model may prevent users from modifying the model to better represent the system at hand. To preserve the flexibility of the fuel cell model, an alternative process evaluation technique, known as pinch analysis [12], is used to determine the magnitude of the heat recovered in the fuel cell system equipment. Pinch analysis computes the maximum amount of thermal energy that may be transferred between the hot and cold streams regardless of the arrangement used to accomplish the heat transfer. Consequently, a model based on pinch analysis is sufficiently generic to model different fuel cell systems without requiring modification. However, the magnitude of heat recovery predicted using pinch analysis represents the theoretical upper limit for heat recovery, and the actual amount of heat recovery accomplished in a heat recovery network will be lower.

In pinch analysis, all of the processes requiring heating are consolidated into a single composite temperature–enthalpy curve that represents the total system heating requirement at each temperature. Similarly, all of the processes requiring cooling and hot exhaust streams undergoing heat recovery are consolidated into a single composite curve that represents the total system cooling requirement at each temperature. Since enthalpy is a relative measure, it is possible to place the two composite curves on a single temperature–enthalpy plot and the curves may be shifted to ensure that the minimum temperature difference is maintained throughout the process temperature range. Thus, using the pinch analysis method, it is possible to determine the theoretical upper limit for heat recovery between the streams in a fuel cell system

that require heating, and the streams that require cooling. Additionally, the fuel processor auxiliary heating requirement, the amount of surplus heat transferred to the cooling water, and the fuel cell auxiliary cooling requirement can be estimated.

Since the heat recovery model permits adjustment of the minimum temperature difference used in the pinch analysis, the model can be modified to reflect a less than ideal performance of an actual heat-recovery system.

4. Validation

Judkoff and Neymark [10] have proposed three validation methodologies for identifying internal errors and for demonstrating that building system models accurately represent the relevant physical systems:

analytical validation involves comparing model predictions to a well known analytical solution for a simplified system,
empirical validation involves comparing model predictions to measured data from the modelled system; and
comparative testing involves comparing model predictions to the predictions made by other models for identical systems.

A test case suitable for analytical validation of the PFCCM system model was not identified. However, elements of the model were validated using both empirical validation and comparative testing methodologies.

4.1. Emperical validation

Very little published data describing the part-load characteristics of operating fuel cell systems exist, and a dataset suitable for validating the PFCCM was not identified. However, numerous studies have published data describing the electrochemical performance of PEM fuel cell stacks. Amongst these, part-load performance dataset published by General Motors [8] was selected to demonstrate the accuracy of the PFCCM's electrochemical model.

Since the PFCCM's electrochemical model is parametric in nature, it is unreasonable to expect the PFCCM to accurately determine the electrochemical performance of a wide range of systems using a generic set of values for the required inputs (α and P_{max}). Therefore, the objective of this empirical validation study was to demonstrate that given an accurate set of inputs describing the fuel cell stack behavior, the PFCCM can accurately predict the performance of a variety of typical PEM fuel cell stacks.

The electrochemical model of the PFCCM was validated by (i) determining parameters (α and P_{max}) from the published experimental data, (ii) using the PFCCM electrochemical model to predict the part-load behavior of the experimental fuel cell stacks, and (iii) comparing the PFCCM part-load performance predictions to the experimental data.

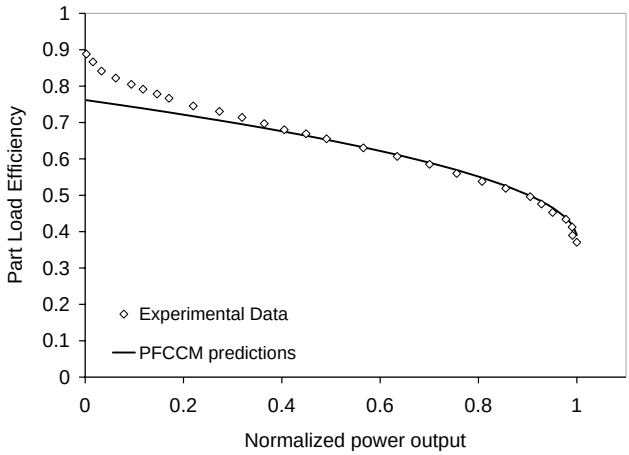

Fig. 3. Comparison of experimental data [8] and PFCCM estimates of part-load efficiency.

A complete discussion of the validation study is available in Ferguson [5].

The part-load efficiency for one experimental fuel cell stack published by General Motors is plotted in Fig. 3, along with the PFCCM electrochemical estimates. Agreement between the PFCCM electrochemical model and the empirical data is excellent at operating points between 20 and 100% of the maximum electrical power. The PFCCM underpredicts the part-load efficiency at power levels below 20%, and the error in the model predictions increases as the power output approaches zero. This disparity results from the assumption that activation polarization losses are constant over the operating range when, in fact, they decrease towards zero at low power levels. Since cogeneration PEM fuel cell systems are typically not operated at turndown ratios of less than 1/5 [11], the operating range between 20 and 100% maximum power is of greatest interest. Disagreement between the PFCCM and experimental data is negligible in this region.

4.2. Comparative testing

The accuracy of the PFCCM's thermal and heat recovery models was assessed by comparing its estimates to those obtained in separate modelling studies conducted by General Motors [7,8] and Beausoleil-Morrison et al. [2].

In support of the General Motors automotive fuel cell research program, researchers at Los Alamos Laboratories developed an Electrochemical Engine System model (ECESYS) to predict the behavior of fuel cell power plants. ECESYS is a proprietary steady-state model that can predict energy and mass flows through the reactors of a fuel cell system at a given operating point [7,8].

To ensure that the PFCCM results could be legitimately compared to the published ECESYS results, the PFCCM was configured using data published in General Motors ECESYS reports. In some instances, the data presented in the General Motors reports were insufficient to determine all of the

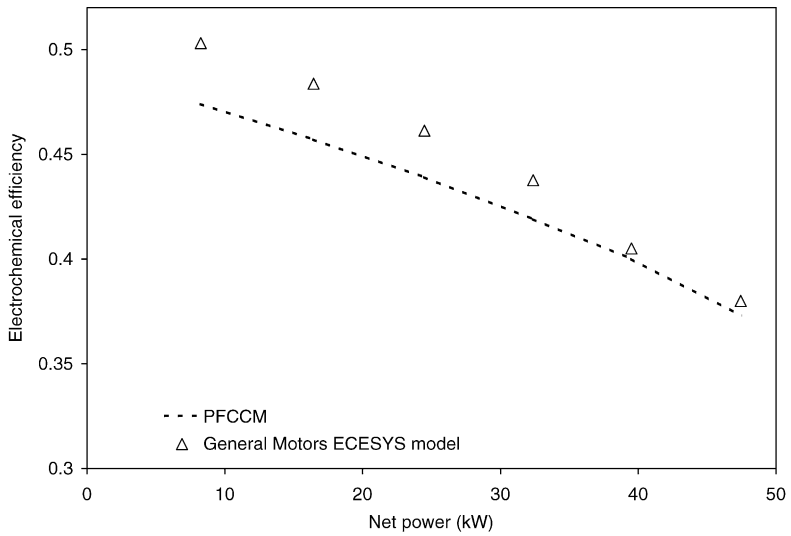

Fig. 4. Comparison of electrochemical efficiency estimates, PFCCM and General Motors ECESYS models.

required parameters, and typical values identified in the literature were used instead.

The PFCCM electrical efficiency estimates are plotted alongside ECESYS predictions in Fig. 4. The average and maximum differences between selected ECESYS and PFCCM predictions are also summarized in Table 1.

Agreement between the PFCCM and ECESYS models was found to be generally very good. However, the PFCCM rejected heat predictions are approximately 80% larger than the ECESYS model predictions. The disparity between the rejected heat predictions is surprising considering the agreement achieved in other aspects of the model performance and may be attributed to differences in the treatment of convective and radiative heat transfer from fuel cell stack in the two models, However, the data provided in the General Motors Reports were insufficient to permit further refinement of the PFCCM estimates.

To the extent that the PFCCM could be configured to represent the fuel cell system modelled in the General Motors modelling study, the PFCCM estimates agree with the published ECESYS results. The differences between the estimates of gross power, electrical efficiency, fuel flow, air flow, and compressor load are small and suggest that the PFCCM may be used with confidence. The large disparity between the cooling load estimates is notable, but too little is known about the structure and configuration of the ECESYS model to attribute these differences to error in the PFCCM.

Table 1
Relative difference between predictions made by ECESYS and PFCCM models (%)

Estimate	Average	Maximum
Gross power	2.4	3.3
System efficiency	3.9	5.8
System fuel flow	4.1	6.1
System air flow	2.4	4.2
Compressor load	2.9	3.8
Rejected heat	76.0	88.0

The validity of the heat recovery estimates obtained by the PFCCM was verified by comparing its predictions with the predictions obtained using an empirical model developed by Beausoleil-Morrison et al. [2]. The results of these comparisons indicate that the heat recovery estimates of the PFCCM are accurate. A detailed discussion of this study can be found in Ferguson et al. [6].

5. Fuel cell sizing study

A case study was conducted using the PFCCM to investigate the impact of varying fuel cell size on the performance of a fuel cell cogeneration system in a modern Canadian household. For this purpose, the PFCCM was used to model the performance of a fuel cell cogeneration system in a test house commissioned by the Canadian Centre for Housing Technology (CCHT). The test house is one of two identical houses built to assess the performance of innovative residential energy technologies. The houses were built in 1998 to the R-2000 standard[3] using methods typical of Canadian wood-frame construction. The two-storey houses enclose 210 m of livable area (excluding a full basement) and are representative in appearance, construction, and layout of new tract-built houses on the Canadian housing market. [15]

[3] R-2000 is a standard developed by the Canadian government to promote energy-efficient building practices in residential housing.[13].

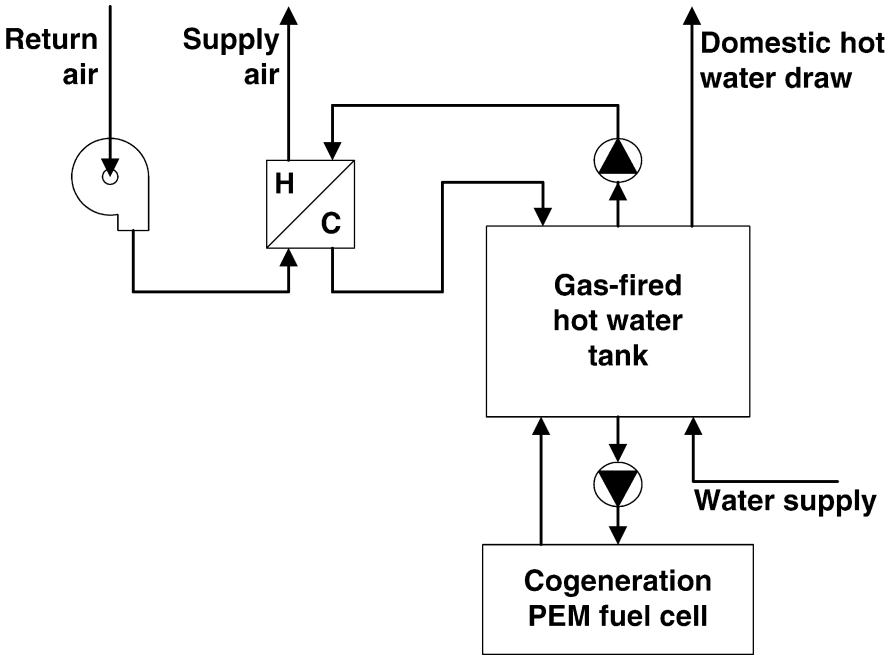

Fig. 5. Arrangement of PEM fuel cell in residential mechanical plant.

In 2001, Purdy and Beausoleil-Morrison [14] constructed a model of one of the CCHT Houses using the ESP-r simulation program. In the ESP-r model, the conditioned living space on the first and second floors in the CCHT house is represented using a single zone. The unheated basement, garage, and attic are represented using separate zones.

In the present study, the CCHT model constructed by Purdy and Beausoleil-Morrison [14] was adapted to include the PEM fuel cell-based mechanical plant depicted in Fig. 5. In this configuration, water from the hot water tank is circulated through the PEM fuel cell system where it is heated using the fuel cell's surplus heat, before it is returned to the tank. Water is also drawn from the tank to (i) supply heat to an air handler that delivers warm air to the conditioned space and (ii) meet the building's domestic hot water loads. The tank is replenished using water provided by the municipal utility.

The hot water tank is equipped with an auxiliary gas burner to ensure that the tank temperature does not fall below 55 °C, the minimum temperature required for effective space heating when the loads on the tank exceed the thermal output of the fuel cell system. The burner is activated when the temperature of the tank drops below 55 °C, and

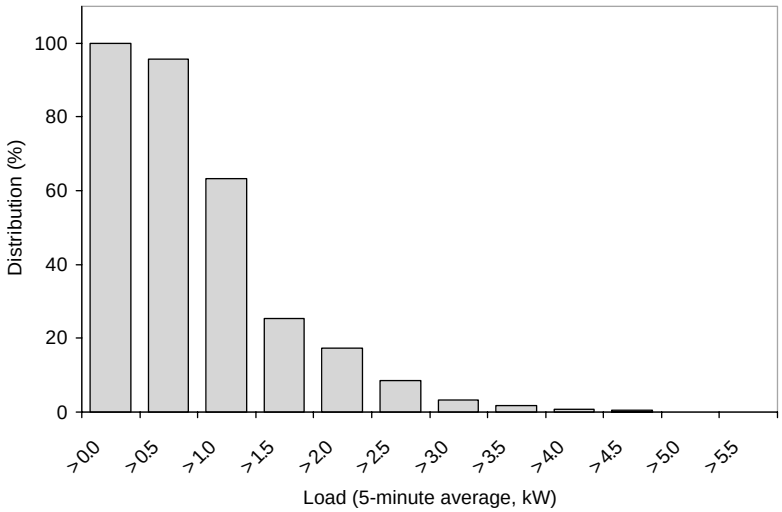

Fig. 6. Distribution of electrical loads.

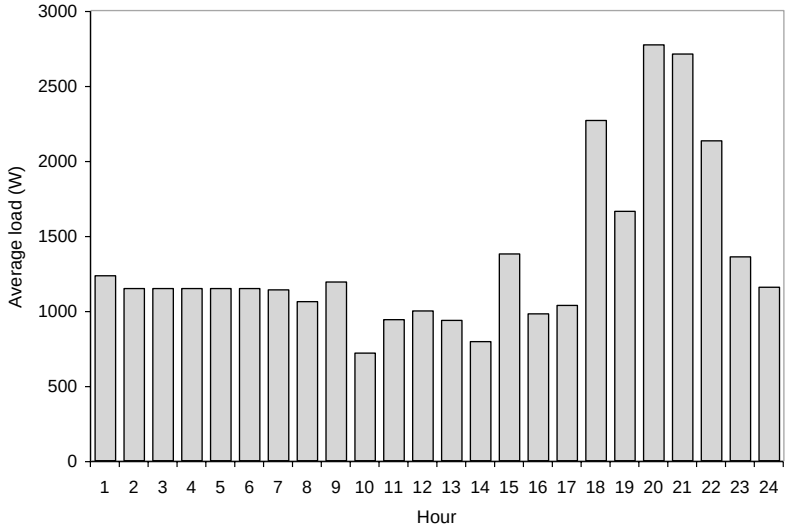

Fig. 7. Hourly average electric load.

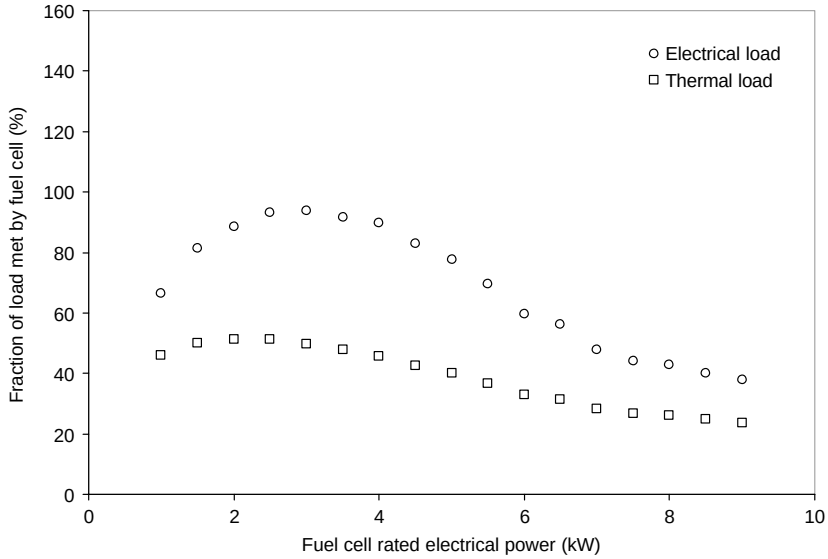

Fig. 8. Impact of fuel cell size on fraction of electrical/thermal loads met by fuel cell, electrical load following scenario.

is deactivated when the temperature rises above 60 °C. The air-handler fan and the pump that supplies the air handler with water are activated when the zone temperature falls below 19.5 °C and deactivated when the zone temperature rises above 20.5 °C. There is no provision to cool the house in the summer months.

The aggregate, occupant-driven electrical loads were described using a profile provided by Kinetrics Inc.[4] The profile describes the annual electrical use of a family of four living in Ontario at a 5-min time resolution. While this profile is realistic, the annual electrical use associated with this profile is 46% larger than the Canadian average [1], and thus represents a high electricity-consuming demographic. The distribution of electrical loads is shown in Fig. 6, and the average hourly load is presented in Fig. 7.

The operation of the fuel cell system was controlled using two different strategies.

Electric load following scenario: In this scenario, the fuel cell system's electric output is matched to the building's electrical demand, if possible. When the electrical demand exceeds the fuel cell's maximum electrical output, the fuel cell system is operated at its maximum operating point, and additional electricity was purchased from the utility grid. When the electrical demand falls below the fuel cell's minimum electrical output, the fuel cell is deactivated.

[4] 800 Kipling Avenue Toronto, Canada. Tel.: +1 416 207 6000. http://www.kinectrics.com.

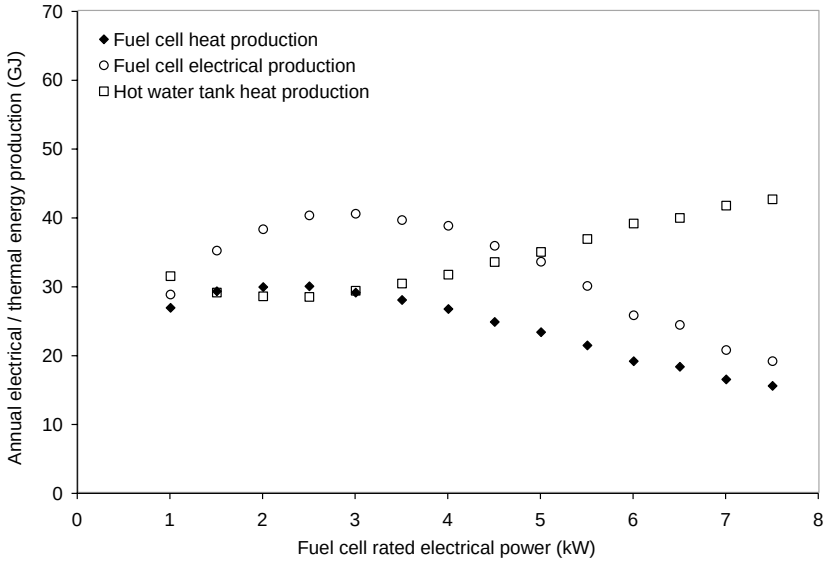

Fig. 9. Impact of fuel cell size on annual electricity/heat production, electrical load following scenario.

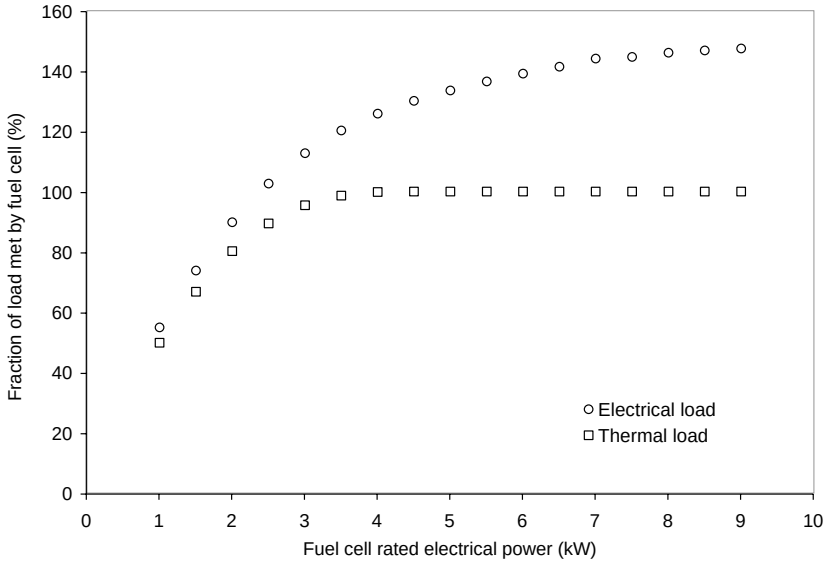

Fig. 10. Impact of fuel cell size on fraction of electrical/thermal loads met by fuel cell, thermal load following scenario.

Thermal load following scenario: In this scenario, the fuel cell system's electrical output is regulated to maintain the hot water tank temperature at a constant 70 °C. Since this temperature is 10 °C above the upper set-point temperature of the hot water tank, the cogeneration plant can meet loads exceeding the fuel cell system's thermal output over extended periods without relying on the hot water tank's auxiliary burner.

In this study, the cogeneration system was not equipped with any electrical storage.[5] A turn down ratio of 1:5 (i.e. minimum output = 20% of maximum output) is typical of residential scale fuel cell systems [11] and was used in this study.

The results of the annual simulations for the electric load following scenario are presented in Figs. 8 and 9, while the results from the thermal load following scenario are presented in Figs. 10 and 11. The fuel cell capacity factor in both configurations is plotted in Fig. 12. As seen in Fig. 8 (fraction of load met by fuel cell), there is a clearly identifiable optimum fuel cell size that maximizes the fraction of the household electrical load met by the

[5] The fuel cell's power conditioning unit, which converts the direct current output of the system into alternating current suitable for use by residential appliances, typically incorporates a small amount of electrical storage permitting it to respond to instantaneous changes in the residential electrical load, while the transient response of the fuel cell is significantly slower. However, the impact of this storage on simulations conducted at a 5-min timestep is negligible.

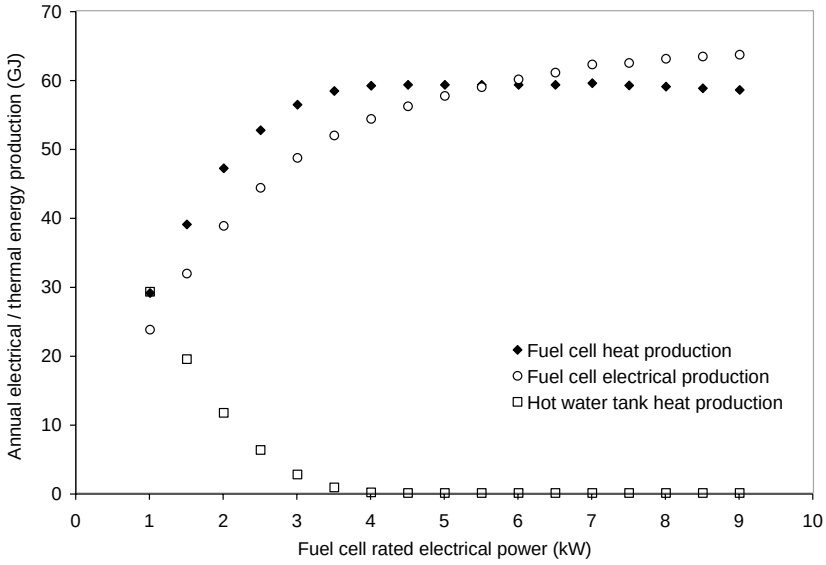

Fig. 11. Impact of fuel cell size on annual electricity/heat production, thermal load following scenario.

fuel cell. For the house considered in the present study, the fuel cell's optimal size is 3 kW, at which point it can provide over 93% of the electricity required within the house.

As the fuel cell size is reduced below this optimum size, the fuel cell does not have sufficient capacity to meet the larger electrical loads in the building. As the fuel cell size is increased, the fuel cell's minimum output also increases, and the fraction of the household load, too small to be met by the fuel cell, grows larger. When the fuel cell is over- or under-sized, the amount of electricity that must be purchased from the utility is larger. The amount of heat produced by the fuel cell is also affected, as shown in Fig. 9, and additional heat must be produced in the hot water tank as the fuel cell size increases.

Figs. 10 and 11 show that the fuel cell's annual electrical and thermal output are substantially larger when the system is configured to meet the building's thermal loads. Similarly, Fig. 12 shows that the fuel cell's capacity factor is larger than that of the electric load following scenario for all sizes larger than 2 kW. When the fuel cell size is increased to 4.5 kW, the system's thermal output is sufficient to meet all of the dwelling's heating requirements and produces 30% more electricity than is required in the dwelling.

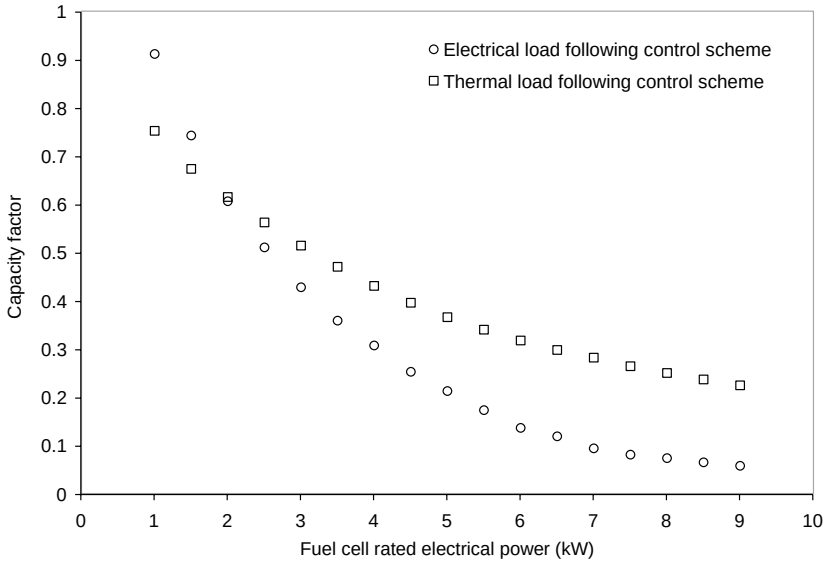

Fig. 12. Impact of fuel cell size on fuel cell capacity factor.

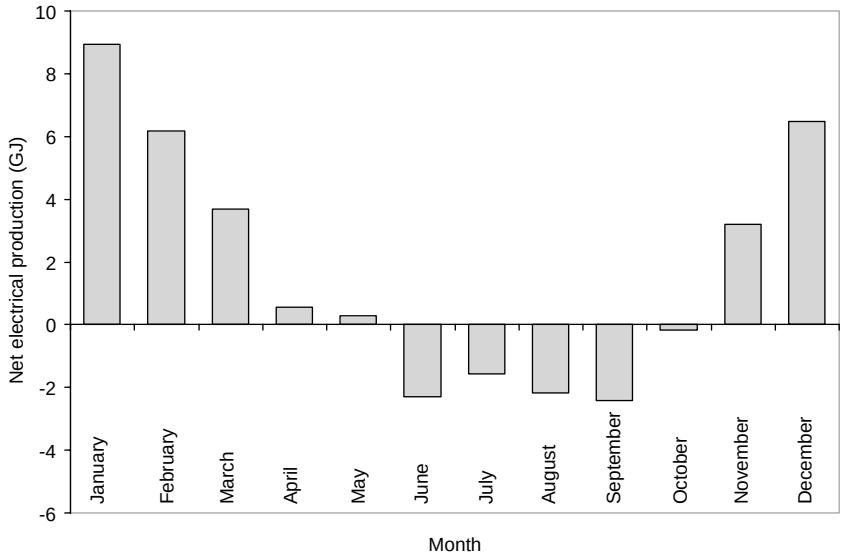

Fig. 13. Monthly electricity balance, 5 kW fuel cell in thermal load following scenario.

While the fuel cell system produces a substantial amount of surplus electricity in the thermal load following configuration, most of this electricity is produced in the winter months, when the thermal demands are highest. Fig. 13 shows the annual monthly electrical balance for a 5 kW fuel cell in the thermal load following scenario. From June to September, the house must import electricity from the electrical grid, while it exports to the grid for the remainder of the year.

These results suggest that (i) in grid-connected applications without electric storage, smaller systems perform better and (ii) fuel cells cannot be deployed in off-grid applications without electric storage unless the system is configured to operate at its minimum output, whenever the actual load is too small for the fuel cell. Since there is no opportunity to export electricity in these applications, it would have to be used on site, perhaps to heat the domestic hot water tank. These results also indicate that the viability of exporting electricity to the grid and the characteristics of electric storage will have an important impact on the feasibility and performance of these systems. Therefore, expanded computer models, capable of simulating the performance of electrical storage and the economics of dispatching electricity to the grid, are required to investigate optimal operating strategies and configurations of these systems.

6. Conclusions

To address the need for a reliable and versatile tool for evaluating the performance of fuel cell cogeneration systems in the building environment, a PEM fuel cell component model (PFCCM) was developed and integrated into the ESP-r building simulation program. The PFCCM is capable of estimating the fuel cell system electricity production, fuel use, and cogeneration heat recovery in response to conditions in the building.

The accuracy of the PFCCM was quantified by comparing its predictions to those made by other fuel cell models and to experimental data. These comparisons indicate that the predictions of the PFCCM are in reasonable agreement with the published data, and from these results, it is concluded that the PFCCM can be used with confidence.

To study the effect of varying fuel cell size on the performance of a cogeneration system, a Canadian case study was conducted using the PFCCM. These results indicate that fuel cell size and operating strategy are critical factors affecting the performance of fuel cell-based cogeneration systems, and further studies and more comprehensive models with the capability of modelling electric storage are necessary to understand the impact of these parameters on the performance of residential fuel cell-based fuel cell cogeneration systems.

Acknowledgements

The authors gratefully acknowledge the financial support provided by the CANMET Energy Technology Centre under the Assistance for Academic Research Supporting CETC's Long-Term Building Simulation Research Objectives program, and by the Natural Sciences and Engineering Research Council of Canada (RGPIN 41739-1999). The authors also gratefully acknowledge the contributions that Ian Beausoleil-Morrison has made to this work.

References

[1] M. Aydinalp, A. Fung, V.I. Ugursal, Household end-use energy consumption in 1997, Technical Report, Canadian Residential Energy End-use Data and Analysis Centre, 2000.

[2] I. Beausoleil-Morrison, D. Cuthbert, G. Deuchars, G. McAlary, The simulation of fuel cell cogeneraion systems within residential

buildings, in: Proceedings of ESim, the Bi-Annual Conference of IBPSA-Canada. IBPSA-Canada, September 2002.
[3] D. Doss, K. Kumar, R. Ahluwalia, M. Krumplet, Fuel processors for automotive fuel cell systems: a parametric analysis, J. Power Sources 102 (2001) 1–15.
[4] M. Ellis, M. Von Spakovsky, D. Nelson, Fuel cell systems: efficient, flexible energy conversion for the 21st century, Proceedings of the IEEE December 2001, 89 (12) (2001) 1808–1818.
[5] A. Ferguson, Fuel cell modelling for building cogeneration applications, Master's Thesis, Dalhousie University, Halifax, Nova Scotia, Canada, February 2003.
[6] A. Ferguson, I. Beausoleil-Morrison, V. Ugursal, A comparative assessment of fuel cell cogeneration heat recovery models, in: Proceedings of Building Simulation 2003, The Eighth International IBPSA Conference, August 2003.
[7] General Motors Corporation, Research and development of proton-exchange-membrane (PEM) fuel cell system of transportation applications, Initial Conceptual Design Report 1994, Republished by Business/Technology Books.
[8] General Motors Corporation, Research and development of proton-exchange-membrane (PEM) fuel cell system of transportation applications, Phase I. Final Report 1996, US Department of Energy Contract no. DE-AC02-90CH10435.
[9] J. Hirschenhofer, Fuel Cell Handbook, Fourth Edition, Federal Energy Technology Center, US Department of Energy, 1998.
[10] R. Judkoff, J. Neymark, International energy agency building energy simulation test (BESTEST) and diagnostic method, Technical Report, National Renewable Energy Laboratory, US Department of Energy, 1995.
[11] T. Kreutz, J. Ogden, Assessment of hydrogen-fueled proton exchange membrane fuel cells for distributed generation and cogeneration, in: Proceedings of the 2000 US DOE Hydrogen Program Review, United States Department of Energy, 2000.
[12] B. Linnhoff, User Guide on Process Integration for the Efficient Use of Energy, Institution of Chemical Engineers, 1994.
[13] Natural Resources Canada, R-2000 technical requirements, Residential Building Energy Standard, Natural Resources Canada, 1994.
[14] J. Purdy, I. Beausoleil-Morrison, The significant factors in modelling residential buildings, in: Proceedings of Building Simulation, 7th International Building Performance Association Conference. IBPSA-Canada, June 2001.
[15] M. Swinton, H. Moussa, R. Marchand, Commissioning twin houses for assessing the performace of energy conserving technologies, in: Proceedings of Exterior Envelopes of While Buildings VIII: Integration of Building Envelopes, December 2001.
[16] B. Thorstensen, A parametric study of fuel cell system efficiency under part-load operation, J. Power Sources 92 (2001) 9–16.
[17] R. Wolk, Fuel cells for homes and hospitals, IEEE Spectrum, May (1999) 45–52.